Bidirectional Q-Z-Source DC Circuit Breaker

Lifang Yi, *Graduate Student Member, IEEE*, and Jinyeong Moon, *Senior Member, IEEE*

***Abstract*—In this article, a novel Z-source dc circuit breaker topology with a Q-shaped impedance network (Q-Z-source circuit breaker) is presented. The new topology has a better performance and is more resilient properties than those of the recently published O-Z-source circuit breaker. The new Q-Z topology provides bidirectional protection but only requires one semiconductor switch in its current path during normal operation, leading to a simpler and smaller physical structure and a lower conduction penalty. It also drastically improves the sensitivity issue on the magnetic coupling coefficient that manifests in the existing O-Z-source circuit breaker. In a realistic, practical application with a nonideal magnetic coupling coefficient, the new topology requires a smaller capacitance that can be translated into lower weight and/or lower cost. Detailed mathematical models are built to analyze and compare the short-circuit fault responses of a variable coupling coefficient. The bidirectional snubber circuit and its connection to the Q-Z topology are discussed for achieving faster fault clearing. Finally, a prototype is built in the laboratory to verify the theoretical analysis and improved performance of the proposed bidirectional Q-Z-source dc circuit breaker.**

***Index Terms*—Bidirectional, breaker, circuit, coefficient, coupling, dc, fault, isolation, microgrid, silicon-controlled rectifier (SCR), thyristor, Z-source.**

I. Introduction

ENVIRONMENTAL issues, such as air pollution and carbon emission, have promoted the rapid development of renewable energy [1], [2]. Most renewable energy sources are in the form of direct current (dc), such as solar photovoltaics. The application of a dc microgrid can effectively reduce the number of power converters, improving the reliability and efficiency of energy transmission. In addition, the dc microgrid can get rid of the issues of harmonic components, synchronization, and reactive power compensation [3], [4]. Thus, dc microgrids have attracted increasing attention in renewable energy systems. However, there are still challenges in the implementation of the dc microgrid, including short-circuit fault protection [5]. When a short-circuit fault occurs on the load side, a huge current surge will follow on the grid side, causing serious damage to the involved systems. The faulty load must be cutoff immediately to protect the systems. However, it is more difficult to isolate a short-circuit fault in the dc grid, compared to the ac grid, due to the absence of a natural zero-crossing point. Traditional electromechanical circuit breakers have a long turn-OFF time and a high probability of an arc occurrence, which is not suitable for the dc microgrid. Therefore, a dc circuit breaker (DCCB) with a fast response time and a reliable isolation capability must be installed between the source and the load to isolate a fault in the dc microgrid and protect the grid participants and subsystems involved.

Semiconductor devices have been adopted in DCCBs for their fast-switching and to achieve arc-free characteristics. Fully controllable semiconductor switches, such as IGBT and IGCT, are used in conventional DCCBs [6], [7]. However, an auxiliary fault-detection circuit with an unavoidable response (delay) time is required to trip a DCCB, resulting in a rather large fault current. The complicated structure and slow response time hinder the wide deployment of conventional DCCBs. In recent years, a novel type of DCCB, called Z-source circuit breaker (ZSCB), is first introduced in [8] to tackle these problems. The ZSCB consists of silicon-controlled rectifiers (SCRs) and *LC* resonance circuits. The Z-source *LC* connection, initially implemented in an impedance-fed inverter, is utilized to handle a fault current interruption in the dc microgrid. When a short-circuit fault occurs, the *LC* network will automatically force the SCR current to cross zero. It automatically cuts off the current path to the faulty load, owing to the automatic shut-off feature of an SCR under zero current without any additional detection circuit.

The ZSCB can be categorized into unidirectional ZSCB (Uni-ZSCB) and bidirectional ZSCB (Bi-ZSCB). Depending on the structure of an *LC* network, Uni-ZSCB can be further divided into three types: cross, parallel, and series structures. They all comprise of one SCR and two sets of *LC* connections and share similar operational principles. In the cross structure, an inductor is inserted between the source ground and the load ground, preventing them from sharing the ground [8], [9]. The parallel structure arranges all components on the same dc bus, realizing the common ground of the load and source [10]. However, a large fault current will directly go through the source. The series structure is proposed to reduce the reflected fault current on the source side by grounding one end of a capacitor [11]. To further reduce the volume and cost, separate inductors can be coupled to form "coupled inductors" [12], [13]. Uni-ZSCB, however, is not always applicable to many dc microgrids if energy transmission is intended for both directions.

Bi-ZSCB is developed to provide bidirectional fault protection. Two SCRs in antiparallel are used to realize bidirectional protection. Two additional diodes or SCRs are conventionally required in the power loop to ensure the correct fault protection,

Manuscript received October 4, 2021; revised January 5, 2022; accepted February 20, 2022. Date of publication February 25, 2022; date of current version April 28, 2022. Recommended for publication by Associate Editor F. Dijkhuizen. *(Corresponding author: Lifang Yi.)*

The authors are with the Department of Electrical Computer Engineering, Florida State University, Tallahassee, FL 32310 USA (e-mail: ly19b@my.fsu.edu; j.moon@fsu.edu).

Color versions of one or more figures in this article are available at https://doi.org/10.1109/TPEL.2022.3153889.

Digital Object Identifier 10.1109/TPEL.2022.3153889

increasing the power loss during the normal operation [14], [15]. The structure of the Bi-ZSCB discussed in [16] is more complicated, consisting of four separated inductors and three capacitors. A simplified structure is built with a single SCR in [17]. However, a full-bridge rectifier is necessary and brings additional power loss. In recent years, Bi-ZSCB is continuously optimized to simplify the structure and improve efficiency. Coupled inductors are also adopted to reduce the volume and weight of Bi-ZSCB and further minimize the required capacitance [18]. In [20], one coupled inductor with a center tap structure is used to replace a three-coil transformer in [19]. The conduction loss of the Bi-ZSCB is still high, owing to the current flowing through at least two semiconductor devices. In [21], the efficiency of the Bi-ZSCB is shown to improve by having only one SCR ON during normal operation. However, four required SCRs in total increase the cost and size, as well as the difficulty in designing driver circuits.

Coupled inductors are also utilized to aid commutation in hybrid dc breakers [22], [23]. One joint terminal of two coupled inductors is connected at one end of the breaker and the remaining two terminals are connected to the semiconductor device and mechanical switch, respectively. When a short-circuit fault occurs, the current through the mechanical switch will be reversed and cross zero due to the coupled inductors. In [24], these coupled inductors are applied to build a Uni-ZSCB with a simple structure. Only two coupled inductors, one SCR, and one capacitor are required. By replacing the single SCR with two SCRs connected in antiparallel, a Bi-ZSCB with an O-shape impedance network (OZSCB) is introduced in [25] recently. Compared with other existing topologies, the OZSCB has fewer components and high efficiency with only one thyristor conducting in the power loop. However, the fault-protection performance of the OZSCB is sensitive to the coupling coefficient of the coupled inductors, which will be discussed in this article. To overcome this issue, a Bi-ZSCB with a Q-shaped impedance network (QZSCB) is proposed in this article. With this modified impedance network, the number of required components still remain the same as the OZSCB, while the required inductance of the QZSCB can be significantly reduced, due to the different internal connections of the coupled inductors. The QZSCB has an advantage in weight and cost. In addition, the QZSCB greatly reduces the sensitivity of the fault-protection performance to the coupling coefficient. When the coupling coefficient is at a practical level (i.e., nonunity) in reality, the capacitance required by the QZSCB is much smaller compared with that of the OZSCB, further reducing the weight and cost. The rest of this article is organized as follows. In Section II, the operational principle of the QZSCB is analyzed. In Section III, the proposed QZSCB is designed and compared with the OZSCB under ideal conditions. The ideal comparison is verified through simulation. Then, the QZSCB and OZSCB are compared with variable coupling coefficients in Section IV. The dynamic response of the fault current is derived with mathematical models. The required capacitances for the QZSCB and OZSCB are obtained and compared when the coupling coefficient is nonunity. The snubber circuit for a faster fault clearing is also covered. A prototype is demonstrated in the laboratory to validate the performance of the QZSCB in Section V. The comparison between the QZSCB and OZSCB is also conducted to verify the correctness of the theoretical analysis. Finally, Section VI concludes this article.

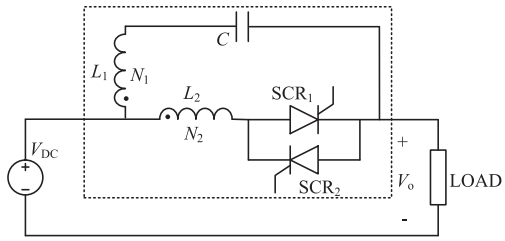

Fig. 1. Circuit diagram of the O-Z-source circuit breaker.

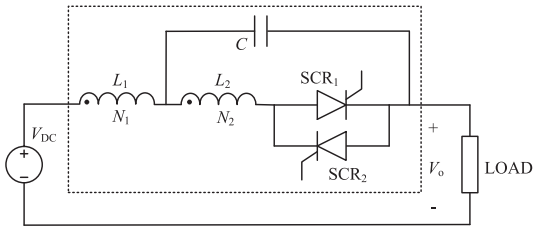

Fig. 2. Circuit diagram of the proposed Q-Z-source circuit breaker.

II. Topology and Qualitative Operating Principle

The topologies of the recently published OZSCB [25] and the proposed QZSCB are shown in Figs. 1 and 2, respectively. They both consist of one capacitor C, two coupled inductors L_1 and L_2, and two SCRs SCR_1 and SCR_2. N_1 and N_2 are the winding turns of L_1 and L_2, respectively. Compared with the OZSCB, the connection of the dotted terminals of L_1 and L_2 is different in the QZSCB. In addition, unlike the OZSCB, L_1 of the QZSCB is placed in the main power loop instead of being in series with C. Their circuit structures are functionally symmetrical from the source end to the load end, naturally ensuring bidirectional protection. In this article, the analysis will be demonstrated on a case where the current flows from left to right. Note that the operational principle in a reverse direction case is the same. The operational principle of the OZSCB is discussed in detail in [25] and summarized here in Fig. 3. The operational principle of the QZSCB, shown in Fig. 4, is discussed in the following.

When the system is in its normal operation, the dc current flows through L_1, L_2, and SCR_1, as shown in Fig. 4(a). The current path is marked red with arrows. Ignoring the voltage drop across L_2 and SCR_1, the capacitor C is completely discharged. The load current is equal to the current through SCR_1 as

$$I_o = I_{\mathrm{SCR}_1} = \frac{V_{\mathrm{dc}}}{R_o} \tag{1}$$

where I_o, I_{SCR_1}, V_{dc}, and R_o denote the load current, current through SCR_1, source voltage of the dc microgrid, and the load resistance, respectively. When a short-circuit fault occurs on the load side, the current path is shown in Fig. 4(b). The load voltage V_o drops from V_{dc} to approximately zero. The capacitor C is

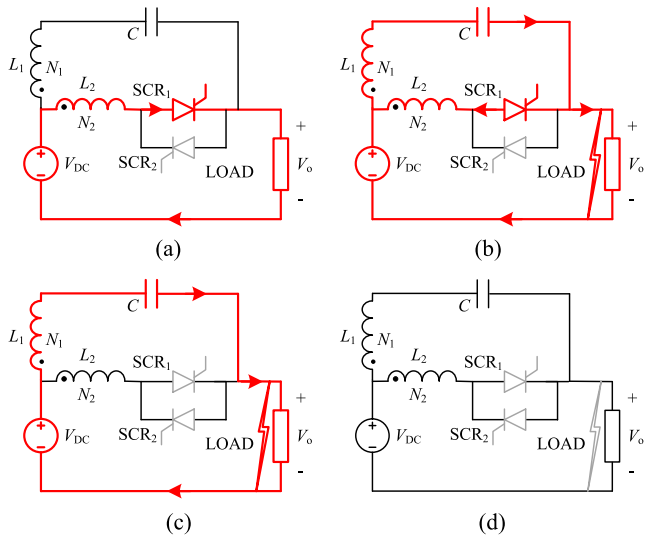

Fig. 3. Operating principle of the OZSCB. (a) Normal operation. (b) Short-circuit fault before SCR is OFF. (c) Short-circuit fault after SCR is OFF. (d) Fault isolation.

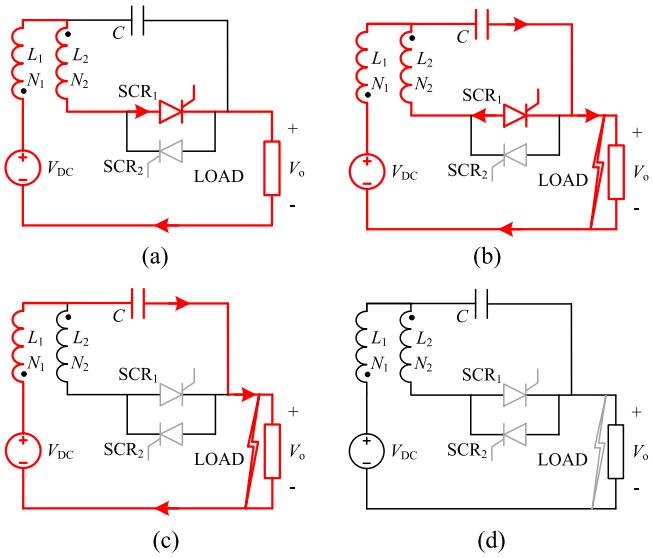

Fig. 4. Operating principle of the QZSCB. (a) Normal operation. (b) Short-circuit fault before SCR is OFF. (c) Short-circuit fault after SCR is OFF. (d) Fault isolation.

charged by the fault current. Due to the rapid rise of the current through L_1, the voltage induced on L_2 generates a transient reverse current, which reduces the initial forward current I_{SCR_1} and makes it cross zero, creating an opportunity to turn itself OFF automatically. SCR_1 will be turned OFF after a short reverse recovery during this time.

After SCR_1 is OFF, L_1 and C continue to resonate, as shown in Fig. 4(c). The fault current decays to zero, in the form of a decaying ac oscillation, due to the loop resistance. A snubber circuit can be used to accelerate the attenuation of the fault current, which will be discussed in the following sections. When the fault current is completely cleared, the short-circuit fault

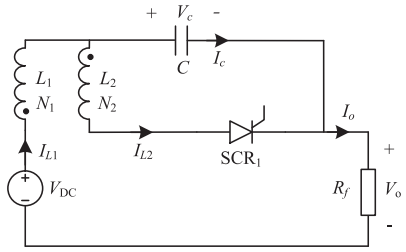

Fig. 5. Equivalent circuit of the QZSCB before SCR is OFF.

is isolated, as illustrated in Fig. 4(d), with no current path remaining. C is charged to the source voltage V_{dc}.

III. Ideal Comparison and Parameter Design

In this section, the fault protection performance of the QZSCB is compared with that of the OZSCB based on the ideal assumptions that

1) The SCR turns OFF as soon as the current crosses zero and it does not suffer from a reverse recovery.
2) The coupling coefficient of L_1 and L_2 is 1.

This is to understand the fundamental differences between the two topologies. Expanding on this knowledge, nonideal effects will be factored in subsequent sections. The turns ratio of the coupled inductor, capacitance, and inductances of the QZSCB and OZSCB are analytically calculated in this section for the same fault-protection performance. The analysis and comparison are verified through simulation.

A. Ideal Parameter Design

1) Turns Ratio $\frac{N_2}{N_1}$: The equivalent load resistances corresponding to the normal operation, short-circuit fault, and maximum allowable load step are defined as R_o, R_f, and R_{step}, respectively. A short-circuit fault can be modeled with a step in load resistance, R_o to R_f. Here, the assumption is that the load voltage is kept constant before the SCR turns OFF. For the QZSCB, the equivalent circuit is shown in Fig. 5. The current through L_1, I_{L1}, is increased by ΔI_{L1}. Since the coupling coefficient is 1, the voltage induced on L_2 reduces the current through L_2, I_{L2}, by ΔI_{L2}, where

$$\begin{cases} \Delta I_{L1} = \frac{V_{\mathrm{dc}}}{R_f} - \frac{V_{\mathrm{dc}}}{R_o} = \frac{V_{\mathrm{dc}}}{R_o}\left(\frac{R_o}{R_f} - 1\right) \\ \Delta I_{L2} = \frac{N_1}{N_2}\Delta I_{L1}. \end{cases} \tag{2}$$

To make sure that SCR_1 can be turned OFF—crossing zero current—ΔI_{L2} should be larger than the initial current as

$$\Delta I_{L2} = \frac{N_1}{N_2}\frac{V_{\mathrm{dc}}}{R_o}\left(\frac{R_o}{R_f} - 1\right) > \frac{V_{\mathrm{dc}}}{R_o}. \tag{3}$$

A similar inequality can be defined for the maximum load step R_{step} for normal operation—without triggering protection

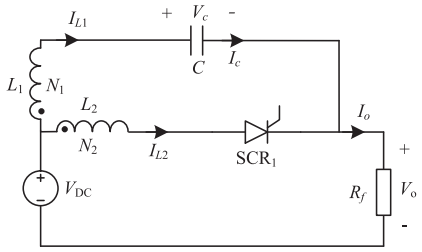

Fig. 6. Equivalent circuit of the OZSCB before SCR is OFF.

as

$$\Delta I_{L2} = \frac{N_1}{N_2}\frac{V_{\text{dc}}}{R_o}\left(\frac{R_o}{R_{\text{step}}} - 1\right) < \frac{V_{\text{dc}}}{R_o}. \tag{4}$$

Combining (3) and (4), the constraint on the turns ratio can be obtained as

$$\frac{1}{m_{\text{step}}} - 1 < \frac{N_2}{N_1} < \frac{1}{m_f} - 1 \tag{5}$$

where $m_{\text{step}} = R_{\text{step}}/R_o$, $m_f = R_f/R_o$.

For the OZSCB, the equivalent circuit is shown in Fig. 6. ΔI_{L1} and ΔI_{L2} during a fault can be written as

$$\begin{cases} \Delta I_{L1} - \Delta I_{L2} = \frac{V_{\text{dc}}}{R_f} - \frac{V_{\text{dc}}}{R_o} \\ \Delta I_{L2} = \frac{N_1}{N_2}\Delta I_{L1}. \end{cases} \tag{6}$$

Combining (6) with an inequality for normal operation, the turns ratio of the OZSCB should satisfy

$$\frac{1}{m_{\text{step}}} < \frac{N_2}{N_1} < \frac{1}{m_f}. \tag{7}$$

Comparing (5) and (7), the turns ratio of the QZSCB is 1 less than that of the OZSCB to achieve the same fault protection range. Defining the winding turns of L_1 and L_2 in the QZSCB as N_a and N_b, respectively, for a given m_{step}, the turns ratios of the QZSCB and OZSCB are

$$\begin{cases} \left[\frac{N_2}{N_1}\right]_{\text{QZSCB}} = \frac{1}{m_{\text{step}}} - 1 = \frac{N_b}{N_a} \\ \left[\frac{N_2}{N_1}\right]_{\text{OZSCB}} = \frac{1}{m_{\text{step}}} = \frac{N_b + N_a}{N_a}. \end{cases} \tag{8}$$

Thus, the maximum allowable load step current I_{step} can be expressed as

$$I_{\text{step}} = \frac{I_o}{m_{\text{step}}} = I_o\left(\frac{N_b}{N_a} + 1\right). \tag{9}$$

The winding turns of the coupled inductors can be adjusted to meet the requirement of a fault protection range, as shown in Fig. 7. Only when the load current is larger than I_{step}, it is possible to trigger the circuit breaker; otherwise, the circuit breaker will never be falsely triggered regardless of the levels of the capacitance and current ramp rate.

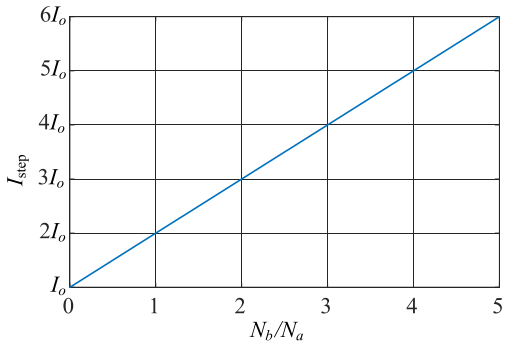

Fig. 7. Maximum allowable load step current with different N_b/N_a.

2) Capacitance C: Capacitor C is charged during the fault protection. The value of capacitance determines whether the current through the SCR can cross zero. For the QZSCB, the charge current of C, ΔI_c, can be expressed as

$$\begin{cases} \Delta I_c = C\frac{dV_C}{dt} \\ \Delta I_c = \Delta I_{L1} + \Delta I_{L2} = \left(1 + \frac{N_2}{N_1}\right)\Delta I_{L2} \end{cases} \tag{10}$$

where V_C denotes the voltage across the capacitor C. Since ΔI_{L2} should be larger than V_{dc}/R_o, the capacitance should satisfy

$$C > \left(1 + \frac{N_2}{N_1}\right)\frac{V_{\text{dc}}}{R_o}\Big/\frac{dV_C}{dt}. \tag{11}$$

If the load voltage collapses at a rate of S_o during a short-circuit fault, the QZSCB's capacitor voltage must increase at a proportional rate based on its KVL.

$$\frac{dV_C}{dt} = \frac{N_2}{N_1 + N_2}S_o. \tag{12}$$

Combining (8), (11), and (12), the minimum required capacitance for the QZSCB is

$$[\text{C}]_{\text{QZSCB}} = \frac{(1 + N_b/N_a)(N_a + N_b)}{N_b S_o}\frac{V_{\text{dc}}}{R_o}. \tag{13}$$

For the OZSCB, ΔI_c is equal to ΔI_{L1} as L_1 and C are in series

$$\begin{cases} \Delta I_c = C\frac{dV_C}{dt} \\ \Delta I_c = \Delta I_{L1} = \frac{N_1}{N_2}\Delta I_{L2}. \end{cases} \tag{14}$$

Thus

$$C > \frac{N_2}{N_1}\frac{V_{\text{dc}}}{R_o}\Big/\frac{dV_C}{dt}. \tag{15}$$

Based on KVL

$$\frac{dV_C}{dt} = \frac{N_2 - N_1}{N_2}S_o. \tag{16}$$

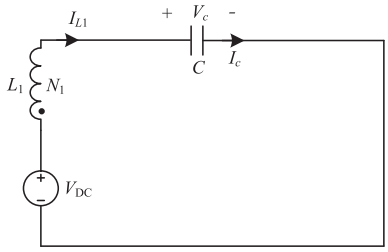

Fig. 8. Simplified equivalent circuit of the QZSCB/OZSCB after SCR_1 is OFF.

Combining (8), (15), and (16) and using the turns ratio from the previous section for the same protection range, the minimum required capacitance for the OZSCB is

$$[\mathrm{C}]_{\mathrm{OZSCB}} = \frac{(1 + N_b/N_a)\,(N_a + N_b)}{N_b\, S_o} \frac{V_{\mathrm{dc}}}{R_o}. \tag{17}$$

Comparing (13) and (17), it can be concluded that the QZSCB can provide the same protection level as the OZSCB with the same capacitance at a lower turns ratio—smaller magnetics.

3) Inductances: L_1 and C start resonance after SCR_1 is OFF, subject to damping via the fault resistance and equivalent series resistance (ESR) of the components and wiring. The simplified, ideal equivalent circuits of the QZSCB and OZSCB in this phase are the same, as illustrated in Fig. 8. In normal operation before the fault, the current through L_1 is I_o in the QZSCB and zero in the OZSCB. After SCR_1 is OFF, the current through L_2 is cleared in both circuits (i.e., reduced by I_o). Accounting for the direction of the coupling dots and turns' ratios for both topologies in (8), the initial currents through L_1 of the QZSCB and OZSCB at the start of the resonance can be shown to be identical as

$$I_{L1}(0) = \left(1 + \frac{N_b}{N_a}\right) I_o. \tag{18}$$

With the zero initial energy in C at the start of this phase (i.e., $V_C(0) = 0$)

$$\begin{cases} I_{L1}(t) = \sqrt{\frac{V_{\mathrm{dc}}^2\, C}{L_1} + I_{L1}^2(0)}\, \sin\left(\frac{t}{\sqrt{L_1\, C}} + \phi_{L1}\right) \\ V_C(t) = V_{\mathrm{dc}} + \sqrt{V_{\mathrm{dc}}^2 + \frac{I_{L1}^2(0)\, L_1}{C}}\, \sin\left(\frac{t}{\sqrt{L_1\, C}} + \phi_C\right) \end{cases} \tag{19}$$

where ϕ_{L1} and ϕ_C denote the initial phase angles of I_{L1} and V_C, respectively. Thus, the peak fault current $I_{L1,\mathrm{max}}$ is

$$I_{L1,\mathrm{max}} = \sqrt{\frac{V_{\mathrm{dc}}^2\, C}{L_1} + I_{L1}^2(0)}. \tag{20}$$

The peak fault current for both the QZSCB and OZSCB can be, therefore, equally suppressed by the increasing L_1. As this is the likely performance indicator for a circuit breaker, the same L_1 would be used in either method for the same capacitance.

TABLE I
MAIN DESIGN PARAMETERS FOR IDEAL COMPARISON

V_{DC} (V)	R_o (Ω)	m_{step}	$I_{L1,\mathrm{max}}$ (A)	S_o (V/μs)	AL (μH/T^2)
28	10	0.5	11.5	0.28	0.4

TABLE II
PARAMETERS DESIGN FOR IDEAL COMPARISON

	N_2/N_1	C (μF)	L_1 (μH)	N_a	N_b	L_2 (μH)
QZSCB	28/28	40	313.6	28	28	313.6
OZSCB	56/28	40	313.6	28	28	1254.4

Rearranging (20) yields

$$L_1 = \frac{C\, V_{\mathrm{dc}}^2}{I_{L1,\mathrm{max}}^2 - I_{L1}^2(0)}. \tag{21}$$

L_2 is then determined based on the turns ratio and L_1 as

$$\begin{cases} [L_2]_{\mathrm{QZSCB}} = \left(\frac{N_b}{N_a}\right)^2 L_1 \\ [L_2]_{\mathrm{OZSCB}} = \left(\frac{N_b + N_a}{N_a}\right)^2 L_1. \end{cases} \tag{22}$$

If the winding turns of L_1 and L_2 of the QZSCB are N_a and N_b, respectively, as defined previously, then those of the OZSCB should be N_a and $(N_b + N_a)$, respectively, with the same magnetic core.

In summary, for the same protection requirements, the required component values for C and L_1 of the QZSCB and OZSCB are identical. The L_2 required for the OZSCB is larger than that for the QZSCB (i.e., $(N_b + N_a)$ versus N_b). The inductors contained in the normal conduction loop of the QZSCB and OZSCB are different (i.e., L_1 and L_2 for the QZSCB versus L_2 for the OZSCB). However, the number of winding turns in the conduction loop are both $(N_a + N_b)$, leading to the same conduction loss. Based on ideal conditions, the QZSCB and OZSCB are similar in procedures for a parameters design. For the same protection performance, the QZSCB needs a lower inductance, resulting in lower volume, weight, and cost. In the subsequent sections, nonidealities will be factored in to highlight additional advantages in the QZSCB topology.

B. Design Example and Simulation Verification

The QZSCB and OZSCB circuits are built in a circuit simulator with the parameters determined by the procedures outlined above. Circuit parameters are given in Tables I and II. Here, AL represents the inductance factor of the magnetic core, and ideal SCRs are used for SCR_1 and SCR_2. As discussed, for the same protection requirements, the number of turns for N_2 of the QZSCB is lower than the OZSCB (i.e., 28 versus 56), resulting in a much lower L_2 (i.e., $313.6\,\mu\mathrm{H}$ versus $1254.4\,\mu\mathrm{H}$), while both topologies have the same values of C and L_1.

For the short-circuit fault, the load resistance is changed from $10\,\Omega$ to $1\,\mathrm{m}\,\Omega$. The resulting waveforms of the input current I_{L1}, current through the SCR I_{SCR}, and voltage across the capacitor V_C of the QZSCB and OZSCB are illustrated in Fig. 9. Note

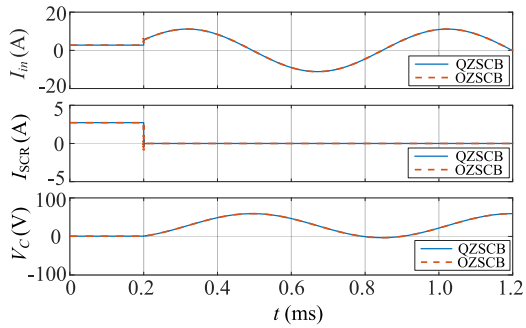

Fig. 9. Simulation of the short-circuit fault for ideal comparison.

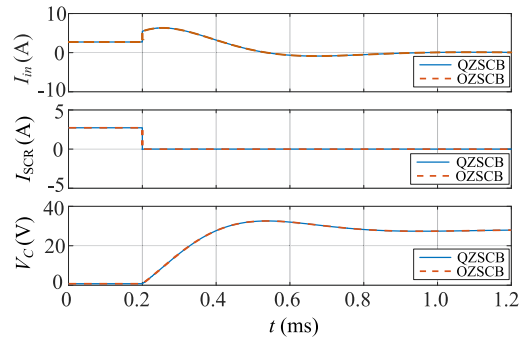

Fig. 10. Simulation of a large load step ($m = 0.33$) for ideal comparison.

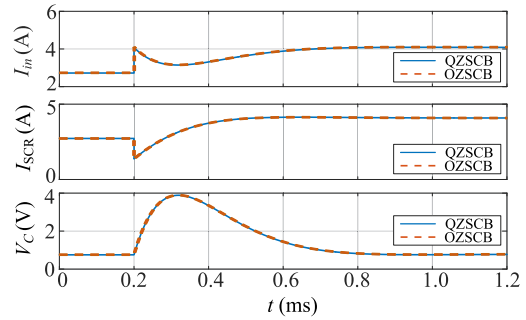

Fig. 11. Simulation of a small load step ($m = 0.66$) for ideal comparison.

that while the SCRs are correctly disengaged after their currents cross zero, this ideal case has negligible damping due to a very minimal loop resistance ($1\,\mathrm{m}\,\Omega$), showing the need for a snubber in such a case. The load step response is also simulated. The fault protection is correctly triggered for a large load step ($m = 0.33$) and correctly remains untriggered for a normal, small load step ($m = 0.66$), as illustrated in Figs. 10 and 11, respectively. The designed target threshold for triggering is at $m = 0.5$. The simulation shows that the resulting waveforms of the QZSCB and OZSCB under different conditions completely overlap with each other, proving the accuracy of the analytical calculations abovementioned and showing the protection characteristics of both topologies.

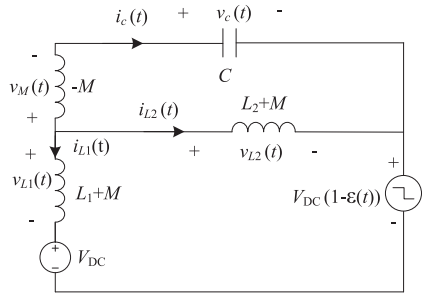

Fig. 12. Equivalent circuit of the QZSCB before SCR is OFF ($k < 1$).

IV. Circuit Model With Variable Coupling Coefficient

The previous section compares the proposed QZSCB with the existing OZSCB in ideal conditions, including the unity coupling coefficient ($k = 1$) of the coupled inductor (i.e., L_1 and L_2). However, the coupling coefficient is less than 1 in reality. In this section, the QZSCB and OZSCB are compared with a variable coupling coefficient. The turn-OFF time of the SCR is also considered for a rigorous comparison. The dynamic response during short-circuit fault protection is analytically derived to calculate the required capacitance for the QZSCB and OZSCB. It is found that the fault protection performance of the OZSCB is more sensitive to the coupling coefficient compared to that of the QZSCB. The capacitance required by the QZSCB is greatly reduced when the coupling coefficient becomes smaller. The QZSCB also provides a much faster protection speed compared to the OZSCB. In addition, the snubber circuit is discussed to speed up the fault clearing. The analysis is verified in simulation.

A. Dynamic Response

Here, the dynamic responses of the QZSCB and OZSCB are derived with a variable coupling coefficient k, expanding on the ideal design process in Section III-A. The mutual inductance between L_1 and L_2, M, is expressed as

$$M = k\sqrt{L_1 L_2}. \tag{23}$$

Ignoring the conduction loss of each component, the equivalent circuit of the QZSCB before SCR_1 is OFF is shown in Fig. 12. A voltage step $\varepsilon(t)$ is introduced on the load side to represent the short-circuit fault. According to KCL and KVL, the relationship between currents and voltages in the time domain can be expressed as

$$\begin{cases} i_{L1}(t) + i_{L2}(t) + i_c(t) = 0 \\ i_c(t) = C\frac{dv_c(t)}{dt} \\ (L_2 + M)\frac{di_{L2}(t)}{dt} = -M\frac{di_c(t)}{dt} + v_c(t) \\ (L_1 + M)\frac{di_{L1}(t)}{dt} = -\varepsilon(t)V_{\mathrm{dc}} + (L_2 + M)\frac{di_{L2}(t)}{dt}. \end{cases} \tag{24}$$

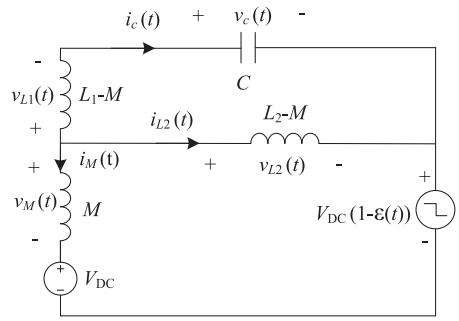

Fig. 13. Equivalent circuit of the OZSCB before SCR is OFF ($k < 1$).

When solved, $i_{L2}(t)$, the current through L_2 and SCR_1 of the QZSCB, is

$$i_{L2,\mathrm{Q}}(t) = \frac{V_{\mathrm{dc}}}{R_o} + \frac{V_{\mathrm{dc}}}{A_L\ (N_a^2 + N_b^2 + 2\,k\,N_a\,N_b)} \times \left[t - A_{\mathrm{Q}}(k)\sin\left(\omega_{\mathrm{Q}}(k)t\right)\right]. \tag{25}$$

"Q" is added in the subscript of i_{L2} to differentiate the QZSCB from the OZSCB. A_{Q} and ω_{Q} are functions of the coupling coefficient. A_{Q} is related to the amplitude of the sinusoidal oscillation and ω_{Q} represents the resonant angular frequency of the equivalent circuit of the QZSCB as

$$\begin{cases} A_{\mathrm{Q}}(k) = \dfrac{1+k^2+\frac{k\left(N_a^2+N_b^2\right)}{N_a N_b}}{\sqrt{\frac{\left(N_a^2+N_b^2+2kN_aN_b\right)(1-k^2)}{C\cdot AL\cdot N_a^2 N_b^2}}} \\ \omega_{\mathrm{Q}}(k) = \sqrt{\dfrac{N_a^2+N_b^2+2kN_aN_b}{C\cdot AL\cdot N_a^2N_b^2(1-k^2)}}. \end{cases} \tag{26}$$

Similarly, the equivalent circuit of the OZSCB before SCR_1 is OFF, as shown in Fig. 13. The current through L_2 and SCR_1 of the OZSCB can be calculated as

$$i_{L2,\mathrm{O}}(t) = \frac{V_{\mathrm{dc}}}{R_o} + \frac{V_{\mathrm{dc}}}{AL\cdot\ (N_a + N_b)^2} \times \left[t - A_{\mathrm{O}}(k)\sin\left(\omega_{\mathrm{O}}(k)t\right)\right]. \tag{27}$$

The expressions of $A_{\mathrm{O}}(k)$ and $\omega_{\mathrm{O}}(k)$ of the OZSCB are different from the QZSCB. When solved

$$\begin{cases} A_{\mathrm{O}}(k) = \dfrac{k\left(1+\frac{N_b}{N_a}\right)-k^2}{\sqrt{\frac{1-k^2}{C\cdot AL\cdot N_a^2}}} \\ \omega_{\mathrm{O}}(k) = \sqrt{\dfrac{1}{C\cdot AL\cdot N_a^2(1-k^2)}}. \end{cases} \tag{28}$$

Referring to (25) and (27), the dynamic responses of both the QZSCB and OZSCB consist of a dc component, linear increment, and sinusoidal component. The coupling coefficient, though, has different effects on the dynamic response of $i_{L2,\mathrm{Q}}(t)$ and $i_{L2,\mathrm{O}}(t)$. It is one of the key factors that determine whether the current through the SCR can drop below zero in the event of a short-circuit fault—ensuring the triggering of the protection.

B. Required Capacitance With Variable Coupling Coefficient

In this section, the influence of k on the dynamic responses is discussed in detail. With the same k, the capacitances required by the QZSCB and OZSCB are derived and compared. Judging from the derived dynamic responses abovementioned, the required capacitances of the QZSCB and OZSCB with a variable coupling coefficient ($k < 1$) are expected to be clearly different from those discussed in Section III-A.

In general, the necessary condition for the DCCB to function in case of a fault is that the current through the SCR must decrease—making the derivative of $i_{L,2}$ negative—and cross zero. With this negative derivative condition applied to (25) and (27), both the QZSCB and OZSCB yield the following inequality:

$$t > \frac{1}{\omega(k)}\arccos\left(\frac{1}{\omega(k)A(k)}\right). \tag{29}$$

Because of the $\arccos$ function, $\omega(k)A(k)$ must not be smaller than 1 to have a solution. Using (26), the explicit expression of $\omega(k)A(k)$ for the QZSCB is

$$\omega_{\mathrm{Q}}(k)A_{\mathrm{Q}}(k) = \frac{1+k^2+\frac{k\,(N_a^2+N_b^2)}{N_a\,N_b}}{1-k^2}. \tag{30}$$

Equation (30) is a monotonically increasing function of k with the minimum value of 1 when $k = 0$. Thus, (29) always has a solution for the QZSCB when $0 \le k \le 1$, regardless of the value of N_a/N_b. With the QZSCB, the SCR can always be effectively turned OFF and the fault can be isolated as there is no limitation on the value of k to realize the protection.

Similar calculations are performed with (28) for the OZSCB as

$$\omega_{\mathrm{O}}(k)A_{\mathrm{O}}(k) = \frac{k(1+N_b/N_a)-k^2}{1-k^2}. \tag{31}$$

This also has to satisfy $\omega_{\mathrm{O}}(k)A_{\mathrm{O}}(k) \ge 1$ to have a solution, yielding

$$k > \frac{N_a}{N_a+N_b} = \frac{1}{1+N_b/N_a}. \tag{32}$$

Unlike the QZSCB, the OZSCB has a minimum requirement for k, which is related to N_a/N_b. The dependence of OZSCB's minimum k, $k_{\min,\mathrm{O}}$, on N_a/N_b is illustrated in Fig. 14. When $N_a/N_b = 1$, the minimum required k is 0.5. If the actual k is less than $k_{\min,\mathrm{O}}$, the OZSCB cannot realize the protection, whereas there is no limitation for the QZSCB in triggering the protection.

In addition to the limitation on k to ensure a negative slope in the SCR current at the onset of a fault, the protection requires a constraint on the minimum turn-OFF time for the SCR. The turn-OFF time of the circuit (t_c)—the duration where the SCR current stays negative—must be larger than the turn-OFF time required by the SCR device (t_q). This can be met with a proper design of a capacitor. For the QZSCB, t_c can be obtained by solving "$i_{L2,\mathrm{Q}}(t) = 0$" based on (25). However, this equation cannot be solved analytically. Our approach is to approximate the sinusoid in (25), "$\sin\left(\omega_{\mathrm{Q}}k\right)$," to a quadratic function since

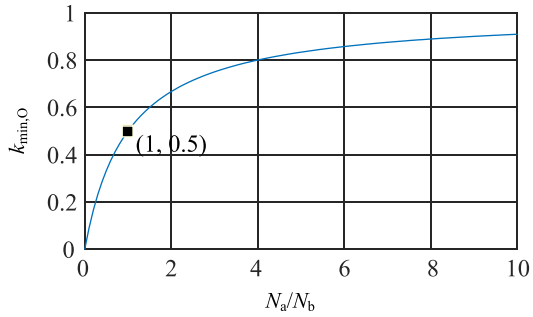

Fig. 14. Minimum allowable coupling coefficient of the OZSCB with different N_a/N_b.

only the first half of the cycle is of interest as

$$\sin(\omega_Q t) \approx -\frac{4}{\pi^2}(\omega_Q t - \pi)\omega_Q t. \tag{33}$$

Substituting (33) into (25) when $0 < \omega_Q t < \pi$, the following equation can be obtained:

$$\omega_Q t^2 - \left(\pi + \frac{\pi^2(k-1)}{4(k+1)}\right)t + \frac{\pi^2 N_a\sqrt{\frac{AL\cdot(2-2k)}{C}}}{2R_o\omega_Q} = 0 \tag{34}$$

where it is assumed that $N_a = N_b$. Please note that a typical setting in the QZSCB (and OZSCB) will be in the vicinity of this design point, hence shown here as a demonstration. By solving (34), the circuit turn-OFF time can be derived from the difference of the two solutions as

$$t_{c,Q} = \frac{\sqrt{\left(\pi + \frac{\pi^2(k-1)}{4(k+1)}\right)^2 - \frac{2\pi^2 N_a\sqrt{\frac{AL\cdot(2-2k)}{C}}}{R_o}}}{\omega_Q}. \tag{35}$$

Applying $t_{c,Q} > t_q$ to (35) for a guaranteed turn-OFF time, the following inequality about t_q is obtained:

$$\frac{4t_q^2}{AL\cdot N_a^2(1-k)}\frac{1}{C} + \frac{4\pi^2 N_a\sqrt{(2-2k)AL}}{R_o}\sqrt{\frac{1}{C}} - \frac{\pi^2(4k-\pi+\pi k+4)^2}{8(1+k)^2} < 0. \tag{36}$$

Thus, the minimum required capacitance of the QZSCB with respect to the variable coupling coefficient for correct SCR turn-OFF and protection trigger can be calculated based on (36) as

$$C_{\min,Q}(k) = \frac{2R_o^2 t_q^4 / \left(\pi^4 AL^3 N_a^6 (1-k)^2\right)}{\left[\sqrt{1-k+\frac{t_q^2 R_o^2(4k-\pi+\pi k+4)^2}{16\pi^2 AL^2 N_a^4(1-k)(k+1)^2}} - \sqrt{(1-k)}\right]^2}. \tag{37}$$

Similarly, the circuit turn-OFF time of the OZSCB can be derived as

$$t_{c,O} = \frac{\sqrt{\left(\pi + \frac{\pi^2(k^2-1)}{4(2k-k^2)}\right)^2 - \frac{4\pi^2 N_a\sqrt{\frac{AL\cdot(1-k^2)}{C}}}{R_o(2k-k^2)}}}{\omega_O}. \tag{38}$$

The minimum required capacitance of the OZSCB with respect to the variable coupling coefficient for correct SCR turn-OFF and protection trigger is

$$C_{\min,O}(k) = \frac{R_o^2 t_q^4 k^2(2-k)^2 / \left(4\pi^4 AL^3 N_a^6 (1-k^2)^2\right)}{\left[\sqrt{1-k^2+\frac{t_q^2 R_o^2(8k-\pi-4k^2+\pi k^2)^2}{64\pi^2 AL^2 N_a^4(1-k^2)}} - \sqrt{(1-k^2)}\right]^2}. \tag{39}$$

In addition, the protection speed of DCCB can be reflected by the time required for the fault current to cross zero. For the QZSCB, the time when the fault current through the SCR crosses zero can be derived based on (34) as

$$t_{1,Q} = \frac{\left(\pi + \frac{\pi^2(k-1)}{4(k+1)}\right) - \sqrt{\left(\pi + \frac{\pi^2(k-1)}{4(k+1)}\right)^2 - \frac{2\pi^2 N_a\sqrt{\frac{AL\cdot(2-2k)}{C}}}{R_o}}}{2\omega_Q}. \tag{40}$$

Similarly, the time when the fault current crosses zero in the OZSCB is

$$t_{1,O} = \frac{\left(\pi + \frac{\pi^2(k^2-1)}{4(2k-k^2)}\right) - \sqrt{\left(\pi + \frac{\pi^2(k^2-1)}{4(2k-k^2)}\right)^2 - \frac{4\pi^2 N_a\sqrt{\frac{AL\cdot(1-k^2)}{C}}}{R_o(2k-k^2)}}}{2\omega_O}. \tag{41}$$

C. Simulation Verification

As an example, the minimum required capacitance with a variable coupling coefficient for the QZSCB and OZSCB are calculated by (37) and (39), respectively, and illustrated in Fig. 15, for an SCR device that requires a minimum turn-OFF time of $t_q = 35\,\mu s$. The SPICE simulation results based on realistic device models are also overlaid, showing an excellent agreement between the calculation and simulation. The calculation and simulation used the same circuit parameters, as given in Tables I and II.

The minimum capacitances required for the QZSCB and OZSCB decrease first and then rise with the increase of k. Thus, a coupling coefficient in the close vicinity of 1, which is difficult to obtain from a practical standpoint, is not desirable from a capacitance perspective either. The variation of $C_{\min,Q}$ is relatively small, which is around several tens of μF. $C_{\min,O}$, on the other hand, is extremely sensitive to k, ranging from several tens of μF to several tens of mF. The ratio of $C_{\min,O}$ to $C_{\min,Q}$ is further provided in Fig. 16. When the coupling coefficient

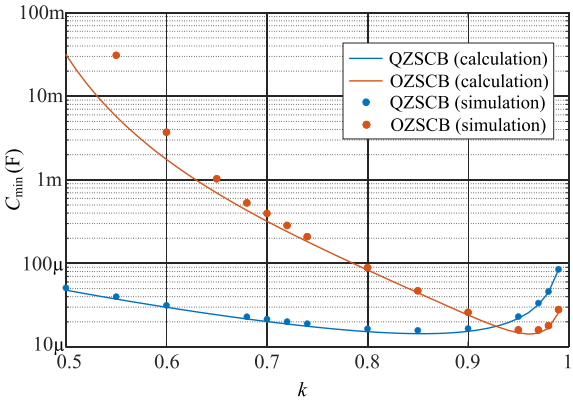

Fig. 15. Minimum required C versus k for the QZSCB and OZSCB ($t_q = 35\,\mu s$).

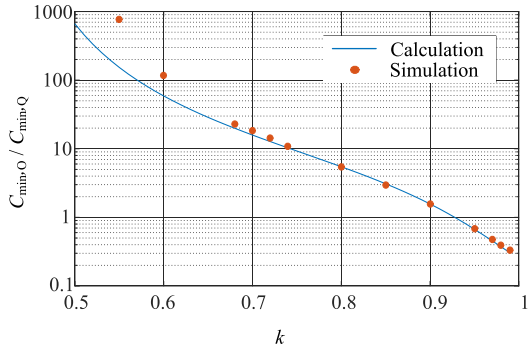

Fig. 16. $C_{\min,O}/C_{\min,Q}$ versus k.

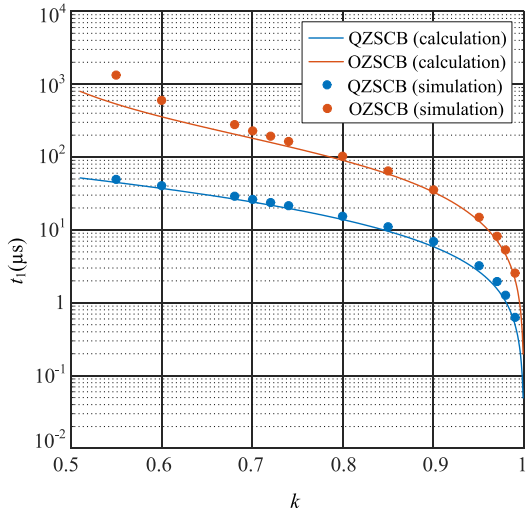

Fig. 17. Protection time of the QZSCB and OZSCB.

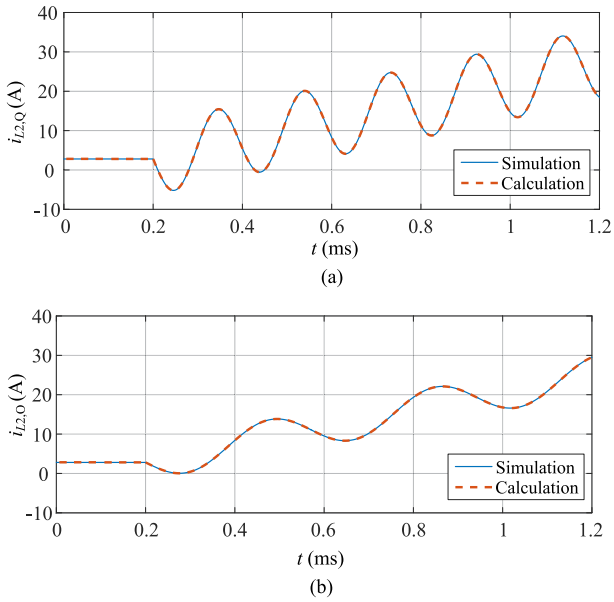

Fig. 18. Dynamic response of i_{L2} in simulation with $k = 0.85$. (a) QZSCB. (b) OZSCB.

is relatively small, $C_{\min,O}$ is much larger than $C_{\min,Q}$. The C required for the OZSCB will be smaller than that for the QZSCB only when k exceeds 0.93. The gaps between the calculation and simulation toward very small k values are due to the approximation of a sinusoid to a quadratic function in (33). The calculation is, otherwise, in excellent agreement with the simulation, effectively validating the influence of the variable coupling coefficient on the required capacitance for the QZSCB and OZSCB and providing an effective design reference for the selection of capacitance.

Based on the minimum required capacitances provided by (37) and (39), the protection times of the QZSCB and OZSCB calculated by (40) and (41), respectively, are provided in Fig. 17 and overlaid with the simulation results. The time required for the OZSCB to force the fault current to cross zero is much longer than that for the QZSCB—the QZSCB can provide much faster protection when a fault occurs.

To verify the dynamic responses of the QZSCB and OZSCB in the time domain, the *LC* structures, shown in Figs. 12 and 13 are simulated and compared with (25) and (27), respectively. Here, used are the same main circuit parameters provided in Tables I and II. Note that SCRs are not considered in the circuits for this comparison and no active/passive damping is applied since this is to validate the dynamic responses associated with the *LC* structures. The coupling coefficient of 0.85 is chosen and the short-circuit fault is injected at $t = 0.2\,\mathrm{ms}$ for both the QZSCB and OZSCB. The simulation results are overlaid with the calculation results as illustrated in Fig. 18, proving the correctness of derived equations. With the same design parameters, the rate at which i_{L2} is decreasing at the onset of a fault ($t = 0.2\,\mathrm{ms}$) is visibly faster in the QZSCB, compared to the OZSCB. This is consistent with the theoretical analysis. In fact, i_{L2} of the OZSCB is not only decreasing slowly but also cannot cross zero. With this set of parameters, the OZSCB will not be able to provide proper fault protection.

Established with the accuracy of the dynamic response model, the DCCB circuits for the QZSCB and OZSCB, including SCRs, are validated in simulation. Using the same circuit parameters provided in Tables I and II, the minimum required capacitance

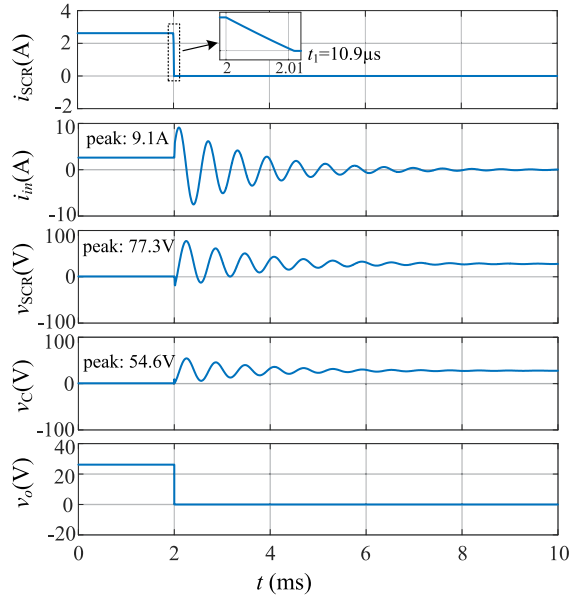

Fig. 19. Short-circuit fault protection of the QZSCB in simulation ($k = 0.85$ and $C = 30\,\mu$F).

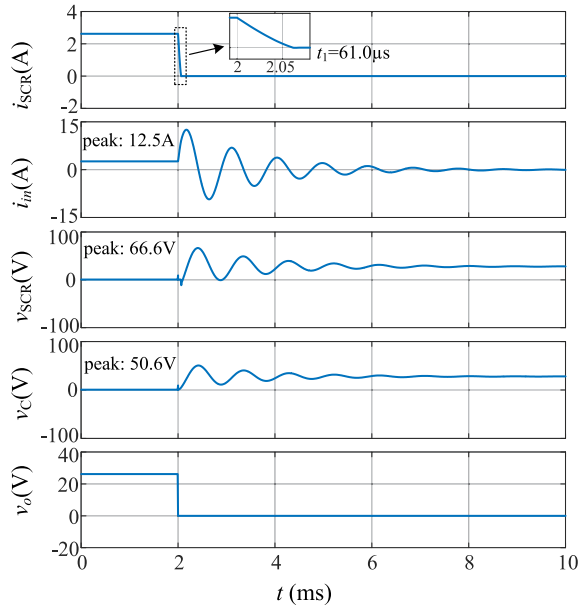

Fig. 20. Short-circuit fault protection of the OZSCB in simulation ($k = 0.85$ and $C = 70\,\mu$F).

is $14.4\,\mu$F for the QZSCB and $44.6\,\mu$F for the OZSCB, according to (37) and (39), under the conditions of $t_q = 35\,\mu$s and $k = 0.85$. In a real application, to ensure effective protection and provide a sufficient margin for unaccounted nonideal effects (e.g., parasitic capacitance, loop inductance and resistance, ESR of components, magnetic loss, etc.), the capacitance can be overestimated by more than 50%. Here, a resistor of $400\,\mathrm{m}\Omega$ is connected in series with the dc power supply, representing the loop resistance in reality. The capacitances of 30 and 70 μH with margin are used for the QZSCB and OZSCB, respectively. The simulated waveforms are shown in Figs. 19 and 20. Both circuits can successfully turn OFF the SCR and isolate the fault (i.e., i_{SCR}s become 0 and stay at zero for both cases). However, as no active/passive damping is reflected in the circuits (e.g., ESR of each component, loop resistance, etc.), L_1 and C will ring for a very long time once it starts resonating when the SCR is OFF, unable to clear a fault in a short time.

D. Snubber Circuit

The voltages of the SCR and capacitor will settle at the input dc voltage (V_{dc}) after successful protection. However, oscillating voltages until they settle require a much higher voltage rating than the input dc level. To alleviate this problem, a metal-oxide varistor (MOV) or a transient-voltage-suppression (TVS) diode can be utilized as a bidirectional snubber to reduce the voltage stress and speed up the clearing of the fault. The breakdown voltage of an MOV or a TVS diode V_{BR} should be larger than the input dc voltage. In [25], an MOV is connected in parallel with the capacitor and significantly reduces the peak voltage of the SCR. The same strategy is applicable to both the QZSCB and OZSCB. For the QZSCB and OZSCB, the peak voltage of the SCR is larger than that of the capacitor, as shown in Figs. 19 and 20. It is, therefore, more beneficial to place the snubber circuit across the SCR.

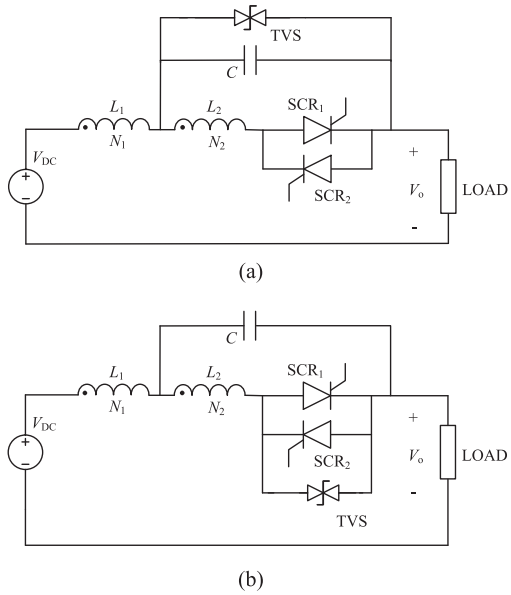

Fig. 21. Snubber circuits of the QZSCB. (a) Snubber across C. (b) Snubber across SCR.

To verify the above-mentioned analysis, a TVS diode is placed across the C or SCR in the QZSCB, as shown in Fig. 21. With the input dc voltage of 28 V, 1N6284 A is chosen as the TVS diode in the simulation, whose break down voltage is 34.2 V. The simulation waveforms of the QZSCB with the snubber circuits are illustrated in Fig. 22, overlaid with the waveforms without the snubber circuits. The peak voltages of the C and SCR are greatly reduced and the fault current quickly decays under the

TABLE III
COMPARISON OF BI-ZSCBS

Category	[14]	[15]	[17]	[18]	[19]	[20]	OZSCB[25]	**QZSCB**
Number of Semiconductor Devices	4	4	5	4	4	4	2	**2**
Number of Magnetic Components	2	2	2	1	1	1	1	**1**
Number of Capacitors	4	3	2	1	1	1	1	**1**
Conducting Devices $(x+y)$[1]	2+2	2+2	3+2	2+2	2+1	2+2	1+1	**1+2**
Common Ground	No	Yes	Yes	Yes	Yes	Yes	Yes	**Yes**
Reflected Fault Current	Zero	High	Moderate	Zero	Zero	Zero	Moderate	**Moderate**
SCR Driver Circuit	Complicated	Simple	Simple	Complicated	Complicated	Simple	Simple	**Simple**
Cost	High	High	High	High	High	High	Moderate	**Low**
Efficiency	Low	Low	Low	Low	Low	Low	Moderate	**High**

[1] x and y represent the numbers of semiconductor devices and inductor coils in the conducting path in normal operation, respectively.

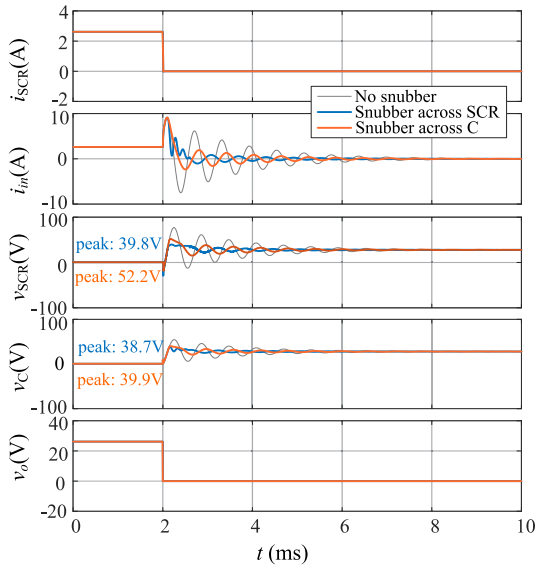

Fig. 22. Simulated fault-clearing waveforms of the QZSCB with the snubber circuit across SCR and C.

presence of the snubber circuit. If the snubber circuit is across the capacitor, the peak voltage of the SCR is 52.2 V. When the snubber circuit is in parallel with the SCR instead, the peak voltage of the SCR is 39.8 V and the fault clearing speed is noticeably faster. Thus, the snubber circuit will be placed across the SCR in the following experiments for better suppression performance.

E. Topology Comparison and Design Guideline

The comparison of the proposed bidirectional QZSCB, OZSCB, and other existing Bi-ZSCBs is given in Table III. The QZSCB and OZSCB have the lowest number of semiconductor devices, magnetic components, and capacitors, simplifying the driver circuit design of SCRs and reducing the cost and weight. Although there is one more coil in the conduction loop of the QZSCB compared to the OZSCB, the total conducting winding turns are identical in principle. Since the required capacitance of the QZSCB is less sensitive to the coupling coefficient and generally smaller than that of the OZSCB for the same peak fault current (20), the inductances in the OZSCB should be increased, resulting in a lower efficiency during normal operation. Small capacitance and inductances ensure the lowest cost and highest efficiency for the proposed QZSCB compared with the existing typologies.

One disadvantage, given in Table III, of the proposed QZSCB, as well as the existing OZSCB, is that a portion of the fault current is reflected to the source. The inductance in the *LC* structure should be selected to limit the peak fault current, as shown in (21). With an appropriate design, the fault-current surges of the QZSCB and OZSCB are tolerable for components in dc microgrids [25].

The parameter design flowchart with a practical coupling coefficient is given as follows.

1) *Ideal estimation:* Based on the design requirements, as given in Table I, the turns ratio of the coupled inductors can be obtained as (8). The required capacitance and inductances are estimated as (13), (21), and (22).
2) *Practical calculation:* The actual coupling coefficient and the required turn-OFF time of the SCR need to be taken into consideration. The minimum required capacitance can be calculated based on (37). Note that (37) is based on the assumption that $N_a = N_b$. When $N_a \neq N_b$, the same analysis steps established in Section IV-B can be followed to get the minimum required capacitance.
3) *Margin and correction:* To enhance the reliability, a certain margin can be padded in capacitance selection based on the calculated minimum value. The inductances can be accordingly adjusted based on the capacitance and the maximum allowable fault current according to (21).

The trigger level will also be affected by the coupling coefficient and the minimum detectable collapse rate of the load voltage, and require further adjustments.

F. Remarks on Applications

The proposed QZSCB is based on a Z-source approach to perform an automatic and fast interruption without active sensing and control in a short-circuit fault condition. However, it may malfunction in load switching and cannot be triggered by a specific current level, similar to other passive circuit breakers, which limits the application. Although the fault-current level is configurable, as discussed in Section III-A, whether the breaker can trip is also determined by the ramp rate of the load current and coupling coefficient. In extreme cases, if the ramp rate of

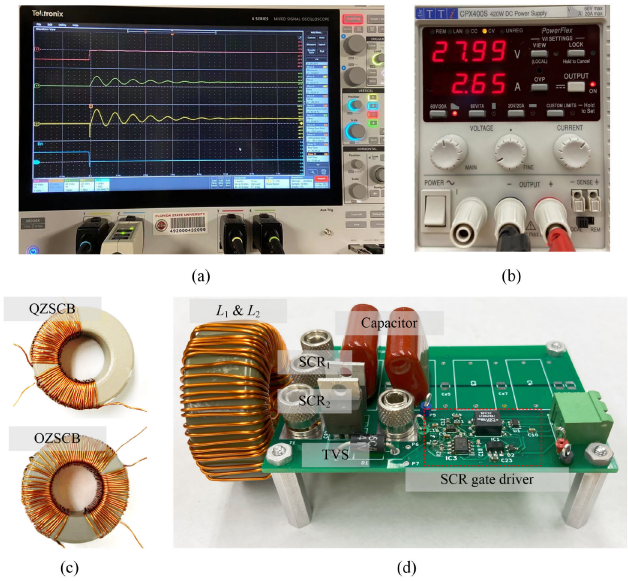

Fig. 23. Experimental platform. (a) Oscilloscope. (b) Power supply. (c) Inductors. (d) DC breaker prototype.

the load step is too slow, the QZSCB may not trigger. In addition, when the external circuit has a non-negligible inductance introduced by cables and filter components, the turns ratio of the coupled inductors and the capacitance should be adjusted [25]. In essence, it can be regarded as the changes in the values of L_1 and M in the equivalent circuit model of the coupled inductors in Fig. 13. More in-depth analyses should follow to consider a nonunity coupling coefficient. Manual tripping circuit [11] and extra fault detection unit [26] can be utilized to help solve this issue and expand the application of passive circuit breakers.

Although a design example at a low-power level is provided in this article, it should be noted that the proposed QZSCB has a competitive advantage in high-voltage and high-current applications. An SCR has a smaller equivalent ON-state resistance and a stronger tolerance to current and voltage surges compared to fully controlled semiconductor devices, such as MOSFET and IGBT. The power losses of the inductors and SCRs in ZSCBs are comparable to other solid-state circuit breakers and only account for a minuscule fraction of the total power in high-power applications [8]. The analysis and parameter design of the circuit components for high-power applications will be largely identical to the low-power level demonstration provided in this article.

V. Experimental Validation

To verify the performance of the proposed topology, a low-voltage experimental platform, shown in Fig. 23, is built. The input dc voltage is 28 V and the load resistance is 10 Ω. The model of the SCR is 2N6403 G with a turn-OFF time of 35 µs. The toroidal magnetic core 58620A2 is used for the coupled inductors with AL of 0.40 µH/T^2. The film capacitor 106MMR100 K is selected for the capacitor C. The TVS diode 1N6284 A is chosen as the snubber circuit across the SCR. The main component parameters are given in Table IV. The coupling

TABLE IV
Component Parameters for Experiments

Component	Parameter	Value
SCR	$I_{T(AV)}$	16 A
	V_{RRM}	400 V
	t_q	35 µs
Coupled Inductors	AL	0.40 µH/T^2
	N_a	28
	N_b	28
	L_1	313.6 µH, $N_1 = 28$
	L_2	QZSCB: 313.6 µH, $N_2 = 28$
		OZSCB: 1254.4 µH, $N_2 = 56$
	k	0.85
Capacitor	C	QZSCB: 30 µF
		OZSCB: 70 µF
TVS	V_{BR}	34.2 V

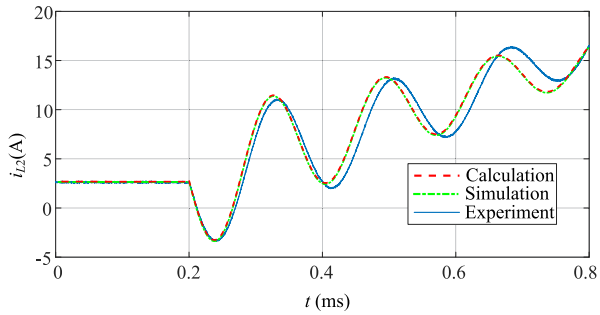

Fig. 24. Dynamic response of i_{L2} of the QZSCB in experiment ($k = 0.85$ and $C = 30$ µF).

coefficients of the coupled inductors of the QZSCB and OZSCB are both measured to be 0.85 by an *LCR* meter. The capacitances are overestimated as 30 and 70 µF for the QZSCB and OZSCB, respectively, consistent with the simulation. Except for the winding and connection structure of the coupled inductors and capacitance, the prototypes of the QZSCB and the OZSCB are identical. The operating mode, whether as the QZSCB or OZSCB, can be configured on our prototype printed circuit board (PCB). The list of equipment used in the experiment is: CPX400S (dc power supply), AFG31000 (function generator), *LCR*-8110 G (*LCR* meter), and MSO64 (oscilloscope).

First, the SCRs and the snubber circuit are removed from the QZSCB circuit to verify the dynamic response of i_{L2} when a short-circuit fault occurs. To prevent a huge current surge without short-circuit fault protection, the current capability of the input power supply is curbed at a reasonable level as a safety measure and the circuit is disengaged before the current level goes beyond the limit. In Fig. 24, the fault happens at $t = 0.2$ ms and the current waveforms of L_2 from the calculation, simulation, and experiment are overlaid. Note that a resistance of 400 mΩ is reflected in the calculation and simulation responses to account for the loop resistance in the experiment, which is measured in the PCB. The equations for the "Calculation" curve are formed by the same previous analysis, but solved in MATLAB for a numerical solution as the explicit solutions

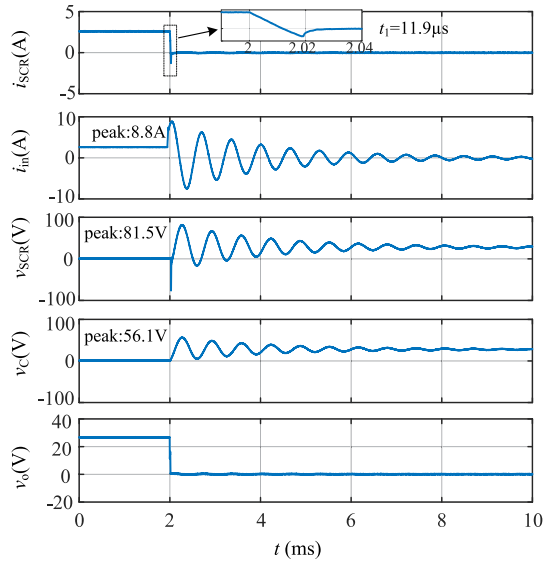

Fig. 25. Short-circuit fault protection waveforms of the QZSCB without the snubber circuit in experiment ($C = 30\,\mu\text{F}$).

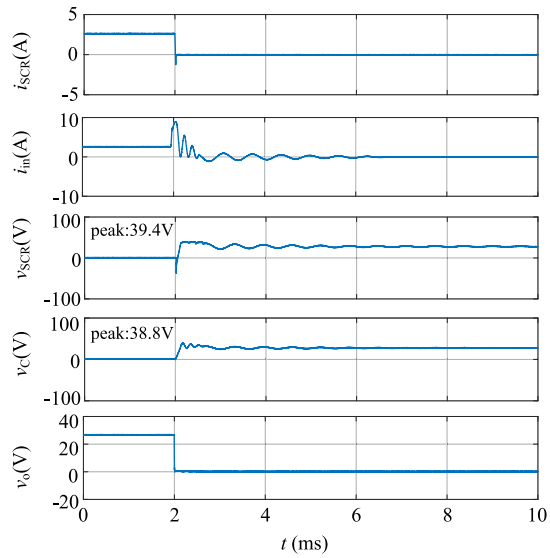

Fig. 26. Short-circuit fault protection waveforms of the QZSCB with snubber circuit in experiment ($C = 30\,\mu\text{F}$).

are difficult to obtain with an additional resistance. The dynamic responses of the calculation and simulation are completely consistent. The corresponding circuit turn-OFF time in the calculation and simulation waveforms is $54.6\,\mu\text{s}$. The circuit turn-OFF time obtained in the experiment is $57.4\,\mu\text{s}$, which is in good agreement with the predicted value in calculation and simulation.

Next, the SCRs are placed back into the circuit. The designed QZSCB is tested with a short-circuit fault without the snubber circuit. The fault clearing waveforms are shown in Fig. 25. When the short-circuit fault happens at $t = 2\,\text{ms}$, the current flowing through L_1, i_{in}, increases sharply, forcing the current through L_2, i_{SCR}, to drop rapidly and cross zero after $11.9\,\mu\text{s}$. The SCR is turned OFF successfully. The oscillation between L_1 and C then starts in the circuit. The peak voltages of the SCR and capacitor are $81.5\,\text{V}$ and $56.1\,\text{V}$, respectively. It validates the operational principle and effectiveness of our QZSCB.

Then, a TVS diode is connected in parallel with the SCR in the QZSCB circuit to perform the short-circuit fault protection. As shown in Fig. 26, the current through the SCR is cut off when the fault happens. Compared with Fig. 25, the *LC* oscillation is greatly attenuated with the snubber circuit, speeding up the fault clearing. The peak voltage of the SCR is reduced from 81.5 to $39.4\,\text{V}$. The peak voltage of the capacitor is reduced from 56.1 to $38.8\,\text{V}$. The experimental result is in good agreement with the simulation, verifying the effectiveness of the snubber circuit.

To make a comparison between the QZSCB and OZSCB, the parameters and connection of the coupled inductors are modified based on Table IV and Fig. 1 to build the OZSCB circuit. The snubber circuit is removed from the circuit and the capacitance is chosen as $30\,\mu\text{F}$, the same as that in the QZSCB. In this case, the short-circuit fault protection is unsuccessful, as shown in Fig. 27. The current of the SCR cannot decrease to zero when the short-circuit fault happens. The fault current cannot be cut off and continues to increase along with the oscillation. Thus,

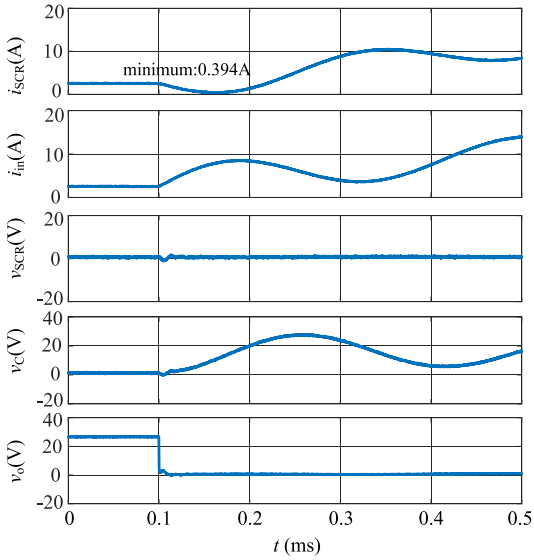

Fig. 27. Short-circuit fault protection waveforms of the OZSCB with the same capacitor $C = 30\,\mu\text{F}$ in experiment.

$30\,\mu\text{F}$ is not enough for the OZSCB to realize short-circuit fault protection, as expected. Based on the calculation and the simulation, the capacitance is increased to $70\,\mu\text{F}$ for the OZSCB and the short-circuit fault protection experiment is repeated. With a capacitor of $70\,\mu\text{F}$, the short-circuit protection is successfully engaged, as shown in Fig. 28. The current through the SCR crosses zero after $51.6\,\mu\text{s}$. The peak voltages of the SCR and the capacitor are $70.6\,\text{V}$ and $53.4\,\text{V}$, respectively.

The short-circuit fault protection of OZSCB with the snubber circuit is also performed, as shown in Fig. 29. The peak voltages of the SCR and the capacitor are reduced and the fault clearing is faster. The experiment of the OZSCB with a capacitor of $60\,\mu\text{F}$ is also carried out in the laboratory. The current through the SCR can cross zero but the SCR cannot be turned OFF due to

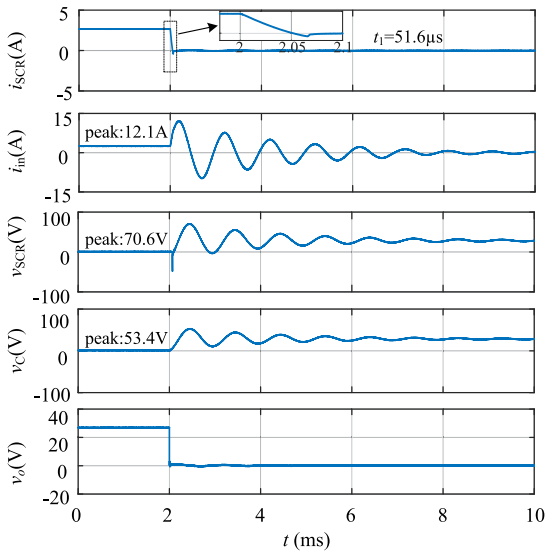

Fig. 28. Short-circuit fault protection waveforms of the OZSCB without snubber circuit in experiment ($C = 70\,\mu$F).

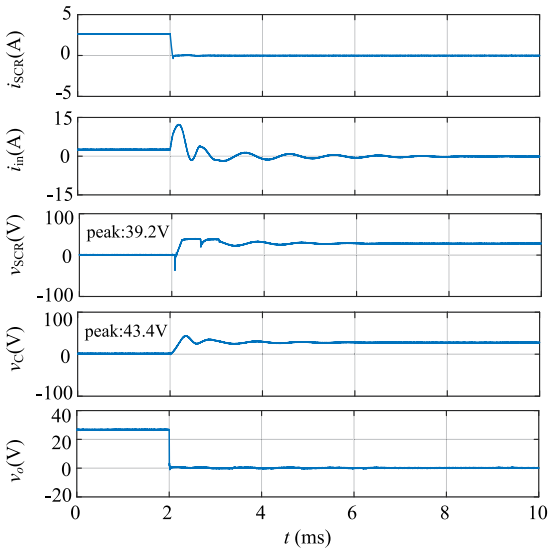

Fig. 29. Short-circuit fault protection waveforms of the OZSCB with snubber circuit in experiment ($C = 70\,\mu$F).

insufficient turn-OFF time. Therefore, the experimental results of the QZSCB and the OZSCB prototypes validate the theoretical analysis, proving that the QZSCB requires less capacitance and ensures faster protection speed than the OZSCB in reality. The short-circuit fault protection is also tested in the reverse direction for the QZSCB and OZSCB. As expected with the symmetry, the reverse direction experiments yield identical response waveforms as Figs. 26 and 29.

VI. Conclusion

In this article, a bidirectional dc circuit breaker with a Q-shaped impedance network is proposed for dc microgrids. The new topology is similar to the existing OZSCB, but has better performance and more resilient properties than the OZSCB. In an ideal case, where the coupling coefficient of the coupled inductor is unity, the QZSCB requires fewer winding turns, showing advantages in weight and cost, compared to the OZSCB, while keeping the required capacitance value the same. Furthermore, in a nonideal, practical case, where the coupling coefficient is less than unity, the dynamic response of the fault current is greatly enhanced. Analyses with a variable coupling coefficient are performed to show that the new topology drastically improves the sensitivity to the magnetic coupling coefficient, compared to the OZSCB. It results in a smaller capacitance for lower weight and cost, especially in lower coupling coefficient cases. The short-circuit protection can be also guaranteed for the QZSCB, unlike the OZSCB, regardless of the coupling coefficient. A bidirectional snubber circuit is considered and applied to the QZSCB and OZSCB. A TVS is adopted and connected in parallel with the SCR for faster fault clearing. A prototype built in the laboratory verified the theoretical analyses and the improved performance of the proposed system, and validated the comparisons between the QZSCB and OZSCB.

References

[1] K. Rahbar, C. C. Chai, and R. Zhang, "Energy cooperation optimization in microgrids with renewable energy integration," *IEEE Trans. Smart Grid*, vol. 9, no. 2, pp. 1482–1493, Mar. 2018, doi: 10.1109/TSG.2016.2600863.

[2] T. Dragičević, X. Lu, J. C. Vasquez, and J. M. Guerrero, "DC microgrids—Part II: A review of power architectures, applications, and standardization issues," *IEEE Trans. Power Electron.*, vol. 31, no. 5, pp. 3528–3549, May 2016, doi: 10.1109/TPEL.2015.2464277.

[3] F. Perez, A. Iovine, G. Damm, L. Galai-Dol, and P. F. Ribeiro, "Stability analysis of a DC microgrid for a smart railway station integrating renewable sources," *IEEE Trans. Control Syst. Technol.*, vol. 28, no. 5, pp. 1802–1816, Sep. 2020, doi: 10.1109/TCST.2019.2924615.

[4] Q. Xu, N. Vafamand, L. Chen, T. Dragičević, L. Xie, and F. Blaabjerg, "Review on advanced control technologies for bidirectional DC/DC converters in DC microgrids," *IEEE Trans. Emerg. Sel. Topics Power Electron.*, vol. 9, no. 2, pp. 1205–1221, Apr. 2021, doi: 10.1109/JESTPE.2020.2978064.

[5] P. Cairoli and R. A. Dougal, "Fault detection and isolation in medium-voltage DC microgrids: Coordination between supply power converters and bus contactors," *IEEE Trans. Power Electron.*, vol. 33, no. 5, pp. 4535–4546, May 2018, doi: 10.1109/TPEL.2017.2724145.

[6] C. Meyer, S. Schroder, and R. W. De Doncker, "Solid-state circuit breakers and current limiters for medium-voltage systems having distributed power systems," *IEEE Trans. Power Electron.*, vol. 19, no. 5, pp. 1333–1340, Sep. 2004, doi: 10.1109/TPEL.2004.833454.

[7] Z. Chen *et al.*, "Analysis and experiments for IGBT, IEGT, and IGCT in hybrid DC circuit breaker," *IEEE Trans. Ind. Electron.*, vol. 65, no. 4, pp. 2883–2892, Apr. 2018, doi: 10.1109/TIE.2017.2764863.

[8] K. A. Corzine and R. W. Ashton, "A new Z-source DC circuit breaker," *IEEE Trans. Power Electron.*, vol. 27, no. 6, pp. 2796–2804, Jun. 2012, doi: 10.1109/TPEL.2011.2178125.

[9] K. Corzine, "DC micro grid protection with the Z-source breaker," *Proc. 39th Annu. Conf. IEEE Ind. Electron. Soc.*, 2013, pp. 2197–2204, doi: 10.1109/IECON.2013.6699472.

[10] K. A. Corzine and R. W. Ashton, "Structure and analysis of the Z-source MVDC breaker," in *Proc. IEEE Electr. Ship Technol. Symp.*, 2011, pp. 334–338, doi: 10.1109/ESTS.2011.5770893.

[11] A. H. Chang, B. R. Sennett, A. Avestruz, S. B. Leeb, and J. L. Kirtley, "Analysis and design of DC system protection using Z-source circuit breaker," *IEEE Trans. Power Electron.*, vol. 31, no. 2, pp. 1036–1049, Feb. 2016, doi: 10.1109/TPEL.2015.2415775.

[12] K. A. Corzine, "A new-coupled-inductor circuit breaker for DC applications," *IEEE Trans. Power Electron.*, vol. 32, no. 2, pp. 1411–1418, Feb. 2017, doi: 10.1109/TPEL.2016.2540930.

[13] W. Li, Y. Wang, X. Wu, and X. Zhang, "A novel solid-state circuit breaker for on-board DC microgrid system," *IEEE Trans. Ind. Electron.*, vol. 66, no. 7, pp. 5715–5723, Jul. 2019, doi: 10.1109/TIE.2018.2854559.
[14] A. Maqsood and K. A. Corzine, "The Z-source breaker for ship power system protection," in *Proc. IEEE Electr. Ship Technol. Symp.*, 2015, pp. 293–298, doi: 10.1109/ESTS.2015.7157907.
[15] D. Keshavarzi, T. Ghanbari, and E. Farjah, "A Z-source-based bidirectional DC circuit breaker with fault current limitation and interruption capabilities," *IEEE Trans. Power Electron.*, vol. 32, no. 9, pp. 6813–6822, Sep. 2017, doi: 10.1109/TPEL.2016.2624147.
[16] S. Savaliya and B. G. Fernandes, "Comparative analysis and coordination study of bi-directional Z-source breaker with reclosing capabilities," in *Proc. 19th Eur. Conf. Power Electron. Appl.*, 2017, pp. P.1–P.10, doi: 10.23919/EPE17ECCEEurope.2017.8099221.
[17] D. J. Ryan, H. D. Torresan, and B. Bahrani, "A bidirectional series Z-source circuit breaker," *IEEE Trans. Power Electron.*, vol. 33, no. 9, pp. 7609–7621, Sep. 2018, doi: 10.1109/TPEL.2017.2764903.
[18] S. G. Savaliya and B. G. Fernandes, "Modified bi-directional Z-source breaker with reclosing and rebreaking capabilities," in *Proc. IEEE Appl. Power Electron. Conf. Expo.*, 2018, pp. 3497–3504, doi: 10.1109/APEC.2018.8341608.
[19] Y. Wang, W. Li, X. Wu, and X. Wu, "A novel bidirectional solid-state circuit breaker for DC microgrid," *IEEE Trans. Ind. Electron.*, vol. 66, no. 7, pp. 5707–5714, Jul. 2019, doi: 10.1109/TIE.2018.2878191.
[20] Y. Yang, C. Huang, Z. Zhao, Q. Xu, and Y. Jiang, "A new bidirectional DC circuit breaker with fault decision-making capability for DC microgrid," *IEEE Trans. Emerg. Sel. Topics Power Electron.*, vol. 9, no. 3, pp. 2476–2488, Jun. 2021, doi: 10.1109/JESTPE.2020.3023653.
[21] Y. Yang and C. Huang, "A low-loss Z-source circuit breaker for LVDC systems," *IEEE Trans. Emerg. Sel. Topics Power Electron.*, vol. 9, no. 3, pp. 2518–2528, Jun. 2021, doi: 10.1109/JESTPE.2020.2986804.
[22] J. Magnusson, L. Liljestrand, and R. Saers, "Apparatus arranged to break an electrical current," U.S. Patent WO2014032692, Mar. 6, 2014.
[23] J. Magnusson, R. Saers, and L. Liljestrand, "The commutation booster, a new concept to aid commutation in hybrid DC-breakers," in *Proc. Cigre Session*, Lund, Sweden, 2015, pp. 1–7.
[24] R. Saers, L. Liljestrand, T. Tengner, and J. Magnusson, "Passive electronic fuse for protecting a DC application," U.S. Patent WO2016198118, Dec. 12, 2016.
[25] Z. Zhou, J. Jiang, S. Ye, D. Yang, and J. Jiang, "Novel bidirectional O-Z-source circuit breaker for DC microgrid protection," *IEEE Trans. Power Electron.*, vol. 36, no. 2, pp. 1602–1613, Feb. 2021, doi: 10.1109/TPEL.2020.3006889.
[26] Z. Zhou, M. Chen, J. Jiang, D. Zhang, S. Ye, and C. Liu, "Analysis and design of a novel thyristor-based circuit breaker for DC microgrids," *IEEE Trans Power Electron.*, vol. 35, no. 3, pp. 2959–2968, Mar. 2020.

Lifang Yi (Graduate Student Member, IEEE) received the B.S. and M.S. degrees in electrical engineering from the Nanjing University of Aeronautics and Astronautics, Nanjing, China, in 2016 and 2019, respectively. She is currently working toward the Ph.D. degree in electrical and computer engineering with Florida State University, Tallahassee, FL, USA.

Her current research interests include precise in-situ magnetic loss measurement, DC circuit breaker, and capacitive wireless power transfer technology.

Jinyeong Moon (Senior Member, IEEE) received the B.S. degree in electrical engineering and computer science from the Korea Advanced Institute of Science and Technology, Daejeon, South Korea, in 2005, the M.S. degree in electrical engineering from Stanford University, Stanford, CA, USA, in 2007, and the Ph.D. degree in electrical engineering and computer science from the Massachusetts Institute of Technology (MIT), Cambridge, MA, USA, in 2016.

From 2007 to 2011, he was a Senior Research Engineer with Hynix Semiconductor, Inc., Icheon, South Korea, where he was involved in designing analog, digital, and power circuits for DDR4 SDRAM. From 2016 to 2017, he was a Postdoctoral Associate with MIT. From 2017 to 2018, he was a member of Technical Staff with Maxim Integrated, North Chelmsford, MA, USA, where he was involved in high efficiency wide bandgap AC–DC converter projects. He is currently an Assistant Professor of electrical and computer engineering with Florida State University. He holds 17 registered U.S. and international patents. His research interests include modeling, design, analysis, and measurement of circuits and systems in the fields of power conversion, energy harvesting, electromagnetics, and renewable energy.

Dr. Moon was the recipient of two grand prizes in the MIT Clean Energy Prize in 2014. He was also the recipient of the Kwanjeong Scholarship and the Hynix Strategic Patent Award. He is currently an Associate Editor for the *Journal of Power Electronics* and the Publication Liaison for IEEE Power Electronics Society's Technical Committee 1.